Journal of Sound and Vibration (1998) **210**(1), 1–18

BIFURCATION AND CHAOS IN A RUB-IMPACT JEFFCOTT ROTOR SYSTEM

F. Chu and Z. Zhang

Department of Precision Instruments, Tsinghua University, Beijing 100084, *People's Republic of China*

(*Received* 26 *May* 1997, *and in final form* 12 *August* 1997)

Non-linear vibration characteristics of a rub-impact Jeffcott rotor are investigated. The system is two-dimensional, non-linear and periodic. Fourier series analysis and the Floquet theory are used to perform qualitative global analysis on bifurcation and stability. The governing ordinary differential equations are also integrated using a numerical method to give the quantitative result. This preliminary study reveals the chaotic feature of the system. After the rub-impact, as the rotating speed is increased, three kinds of routes to chaos are found, that is, from a stable periodic motion through period doubling bifurcation, grazing bifurcation and a sudden transition from periodic motion to chaos. Quasi-periodic motions are also found.

1. INTRODUCTION

Rub-impact between rotor and stator is one of the main serious malfunctions that often occur in rotating machinery. It shows a very complicated vibration phenomenon, including not only periodic (synchronous and non-synchronous) components but also quasiperiodic and chaotic motions. A comprehensive investigation on the dynamic characteristics exhibited by this kind of system forms the basis to diagnose accurately this form of fault.

Rotor-stator rub in a rotating assembly has attracted great concerns from researchers. There have been numerous publications on this topic. Muszynska's literature survey [1] gave a list of previous papers on the rub-related vibration phenomena. She discussed the physical meaning and the thermal effect of rub, various phenomena during rubbing, analysis and vibration response of rubbing rotors, and other related phenomena. Beatty [2] suggested a mathematical model for rubbing forces which were non-linear with a piecewise linear form. The model is still widely used today. Through theoretical simulation and laboratory verification he concluded some points for diagnosing this fault. Choy and Padovan [3] performed a very interesting theoretical investigation to observe the effects of casing stiffness, friction coefficient, imbalance load and system damping on rub force history, and the transient response of rotor orbit. Shaw and Holmes [4] discussed a periodically forced piecewise linear oscillator in a more mathematical way. Their results showed harmonic, subharmonic and chaotic motions. This type of oscillator can be derived from a rub-impact model and the discussion has a representative meaning. Thompson and Stewart [5] studied an impact oscillator. The oscillator is shown to exhibit complex dynamic behaviour including period-doubling bifurcation and chaotic motions. Choi and Noah [6] examined the complex dynamic behaviour of a simple horizontal Jeffcott rotor with bearing clearances. Numerical results have revealed that alternating periodic,

0022–460X/98/060001 + 18 $25.00/0/sv971283

aperiodic, and chaotic responses is governed by the rule of the Farey number tree. There are mode-locking tongues in the parameter space and within each mode-locking tongue, a number of smaller tongues exist where a sequence of period doubling bifurcations leading to chaos takes place. Kim and Noah [7] used a modified Jeffcott model to determine the onset of aperiodic whirling motion using bifurcation theory. Choi and Noah [8] presented a numerical method which combined the harmonic balance method with discrete Fourier transformation and inverse discrete Fourier transformation. Their numerical results showed the occurrence of super- and subharmonics in a rotor model involving a bearing clearance. Chancellor *et al*. [9] discussed a method of detecting parameter changes of a piecewise-linear oscillator using analytical and experimental non-linear dynamics and chaos. Chaotic time series for each of six parameter values was obtained. Movement of the unstable periodic orbits in phase space was used to detect parameter changes in the system. This suggested a possible way for the future fault diagnostics. Muszynska [10] analyzed the physical phenomena related to partial lateral rotor to stator rub. Through using a periodic step function the analysis showed the existence of harmonic vibrations in the order $1/2, 1/3, 1/4, \ldots$; experiment also confirmed the results. Adams and Abu-Mahfouz [11] discussed the chaotic motions of a general rub-impact rotor model. The influence of clearance variation was observed, and responses rich in subharmonic, quasiperiodic and chaotic motions were obtained over a wide range of operating parameters. Ehrich [12] analyzed the rotor dynamic response in non-linear anisotropic mounting systems which represented a rotor system in local contact with the stator. He found the chaotic response in transition zones between successive superharmonic orders. In Isaksson's paper [13], the "jump" phenomenon and the influence of radial clearance were investigated. Recently Chu and Zhang [14] performed a numerical investigation to observe periodic, quasi-periodic and chaotic motions in a rub-impact rotor system supported on oil film bearings. Routes to and out of chaos were analyzed.

The Jeffcott rotor system discussed in this paper is a non-linear vibrating system which includes non-linear rub-impact forces resulting from eccentric rotation of the rotor. The mathematical model is a non-linear and non-autonomous ordinary differential equation. The Fourier series expansion method is used to obtain the analytical expression of the stable periodic solution. Then, the differential equations of perturbation are established based on the perturbation theory, and the Floquet theory is used to analyze the global characteristics of the periodic solutions. A preliminary qualitative analysis is performed. Finally the Runge–Kutta method is used to integrate this non-autonomous system numerically. The preliminary theoretical analysis and numerical calculations reveal the chaotic behaviour of this system. After the rub-impact, as the rotating speed is increased, three kinds of routes to chaos are found, that is, from a stable periodic motion through period doubling bifurcation and grazing bifurcation [15] to chaos, and a sudden transition between periodic vibration and chaos. Quasi-periodic vibrations are also found. These results are of great significance to the effective diagnostics of the rub-impact fault of a rotor system.

2. MATHEMATICAL MODEL

2.1. EQUATIONS OF MOTION

The rub-impact model discussed is a Jeffcott rotor system and is shown in Figure 1. The center of the stator is assumed as the origin of the co-ordinates. Displacements of the disc center are (x, y). The rotor is acted on by gravitation mg, imbalance force induced by

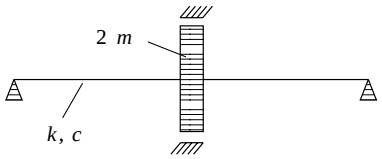

Figure 1. Schematic of the rub-impact rotor system.

U, and, when the rub-impact interaction occurs, the rub-impact forces F_x and F_y. The system can be described by the following differential equations of motion as

$$\begin{cases} m\ddot{x} + c\dot{x} + kx = F_x(x, y) + mU\omega^2 \cos(\omega t) \\ m\ddot{y} + c\dot{y} + ky = F_y(x, y) + mU\omega^2 \sin(\omega t) - mg \end{cases} \tag{1}$$

where c is the damping coefficient of the shaft, k is the stiffness coefficient and U is the imbalance.

2.2. RUB-IMPACT FORCES

It is assumed that there is an initial clearance of δ between rotor and stator. Compared with one complete period of rotating, the time during rub-impact is very short, therefore, an elastic impact model is used. Also the Coulomb type of frictional relationship is assumed in the analysis. When rub happens as shown in Figure 2, the radial impact force F_N and the tangential rub force F_T can thus be expressed as

$$F_N(x, y) = \begin{cases} 0, & (\text{for } e < \delta) \\ (e - \delta)k_c, & (\text{for } e \geqslant \delta) \end{cases} \quad F_T = fF_N$$

where f is the friction coefficient between rotor and stator, k_c, is the radial stiffness of the stator and $e = \sqrt{x^2 + y^2}$ is the radial displacement of the rotor. These two forces can be written in x–y co-ordinates as

$$\begin{aligned} F_x(x, y) &= -F_N \cos\gamma + F_T \sin\gamma \\ F_y(x, y) &= -F_N \sin\gamma - F_T \cos\gamma \end{aligned} \quad \text{or} \quad \begin{Bmatrix} F_x \\ F_y \end{Bmatrix} = H(e - \delta)\frac{(e - \delta)k_c}{e}\begin{bmatrix} 1 & -f \\ f & 1 \end{bmatrix}\begin{Bmatrix} x \\ y \end{Bmatrix} \tag{2}$$

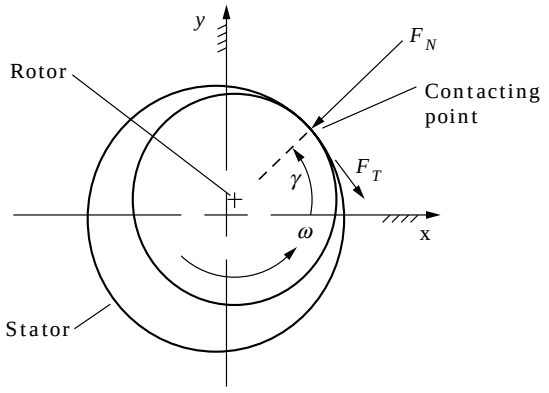

Figure 2. Schematic of rub and impact forces.

where $H: IR \to IR$ is the Heaveside function, that is,

$$H(x) = \begin{cases} 0, & x \leqslant 0 \\ 1, & x > 0 \end{cases}.$$

Equation (2) indicates that when the rotor displacement e is smaller than δ, the static clearance between rotor and stator, there will be no rub-impact interaction and the rub-impact forces are zero while the rub-impacting will happen if the rotor displacement e is bigger than δ.

3. BIFURCATION AND STABILITY ANALYSIS

The Fourier expansion and the Floquet theory are combined to give qualitative analysis of stability and bifurcation for equations (1) and (2). The analysis indicates that there exists a stable periodic solution for this system and this solution shows the period-doubling bifurcation when the rotating speed is increased. First the Fourier expansion can be used to derive the stable periodic solution of the system. Assuming $N\tau = \omega t$, equation (1) can then be written as

$$\begin{cases} x'' = \dfrac{N^2}{m\omega^2} F_x(x, y) - \dfrac{cN}{m\omega} x' - \dfrac{kN^2}{m\omega^2} x + UN^2 \cos N\tau \\ y'' = \dfrac{N^2}{m\omega^2} F_y(x, y) - \dfrac{cN}{m\omega} y' - \dfrac{kN^2}{m\omega^2} y + UN^2 \sin N\tau - \dfrac{gN^2}{\omega^2} \end{cases} \tag{3}$$

where $' = \mathrm{d}/\mathrm{d}\tau$ and N is the subharmonic order. The stable periodic solution of equation (3) is assumed as

$$\begin{cases} x = a_{10} + \sum\limits_{n=1}^{n_s} (a_{1n} \cos n\tau - b_{1n} \sin n\tau) \\ y = a_{20} + \sum\limits_{n=1}^{n_s} (a_{2n} \cos n\tau - b_{2n} \sin n\tau) \end{cases} \tag{4}$$

where n_s is the number of harmonics to be taken into account in the solution. Based on equation (4), $\mathrm{d}x/\mathrm{d}\tau$, $\mathrm{d}y/\mathrm{d}\tau$, $\mathrm{d}^2x/\mathrm{d}\tau^2$ and $\mathrm{d}^2y/\mathrm{d}\tau^2$ can be obtained. Substituting these results into both sides of equation (3), expanding the non-linear terms F_x and F_y on the right side of equation (3) into Fourier series, and comparing coefficients of $\cos(n\tau)$ and $\sin(n\tau)$ on both sides of equation (3) give the following non-linear equations containing $2(2n_s + 1)$ equations:

$$F(\bar{x}) = \{f_0^T, f_{c1}^T, \ldots, f_{sn_s}^T\}^T = 0$$

$$\text{where} \quad \bar{x} = \{a_{10}, a_{20}, a_{11}, a_{21}, b_{11}, b_{21}, \ldots, a_{1n_s}, a_{2n_s}, b_{1n_s}, b_{2n_s}\}. \tag{5}$$

These equations can be written as

$$f_0 = \begin{bmatrix} f_{01} \\ f_{02} \end{bmatrix} = \begin{bmatrix} \dfrac{\alpha}{2\pi} \displaystyle\int_0^{2\pi} F_x \, \mathrm{d}\tau - k\alpha a_{10} \\ \dfrac{\alpha}{2\pi} \displaystyle\int_0^{2\pi} F_y \, \mathrm{d}\tau - k\alpha a_{20} - \dfrac{gN^2}{\omega^2} \end{bmatrix} = 0$$

$$f_{cn} = \begin{bmatrix} f_{cn1} \\ f_{cn2} \end{bmatrix}$$

$$= \begin{bmatrix} n^2 a_{1n} + \dfrac{\alpha}{\pi} \displaystyle\int_0^{2\pi} F_x \cos(n\tau)\, \mathrm{d}\tau - k\alpha a_{1n} + \beta n b_{1n} + UN^2 \delta_{nN} \\ \\ n^2 a_{2n} + \dfrac{\alpha}{\pi} \displaystyle\int_0^{2\pi} F_y \cos(n\tau)\, \mathrm{d}\tau - k\alpha a_{2n} + \beta n b_{2n} \end{bmatrix} = 0, \quad n = 1, 2, \ldots, n_s$$

$$f_{sn} = \begin{bmatrix} f_{sn1} \\ f_{sn2} \end{bmatrix}$$

$$= \begin{bmatrix} -n^2 b_{1n} + \dfrac{\alpha}{\pi} \displaystyle\int_0^{2\pi} F_x \sin(n\tau)\, \mathrm{d}\tau + k\alpha b_{1n} + \beta n a_{1n} \\ \\ -n^2 b_{2n} + \dfrac{\alpha}{\pi} \displaystyle\int_0^{2\pi} F_y \sin(n\tau)\, \mathrm{d}\tau + k\alpha b_{2n} + \beta n a_{2n} + UN^2 \delta_{nN} \end{bmatrix} = 0, \quad n = 1, 2, \ldots, n_s$$

where $\alpha = (N^2/m\omega^2)$ and $\beta = (cN/m\omega)$. The Inverse-Broyden Rank 1 method is used to solve equation (5). The formulae for deriving the solution are

$$\begin{cases} \bar{x}^{k+1} = \bar{x}^k - B_k F(\bar{x}^k) \\ B_{k+1} = B_k + \dfrac{(S^k - B_k Y^k)(S^k)^T B_k}{(S^k)^T B_k Y^k}, \end{cases} \quad \text{and} \quad k = 0, 1, 2, \ldots$$

where $Y^k = F(\bar{x}^{k+1}) - F(\bar{x}^k)$, $S^k = \bar{x}^{k+1} - \bar{x}^k$. Thus equation (4), the stable periodic solution, can be obtained.

Next equation (3) is perturbed, that is, let $x(t) = x_0 + \Delta x(t)$, $y(t) = y_0 + \Delta y(t)$ (where $x_0(t)$ and $y_0(t)$ are the stable periodic solutions obtained above using the Fourier expansion) and substitute these expressions into equation (3). The non-linear terms in equation (3) are expanded into the Taylor series at the point $(x_0(t), y_0(t))$. Retaining the linear terms gives

$$\begin{cases} \Delta\ddot{x} = \alpha\left(\dfrac{\partial F_x}{\partial x} - k\right)\Delta x + \alpha \dfrac{\partial F_x}{\partial y} \Delta y - \beta \Delta\dot{x} \\ \\ \Delta\ddot{y} = \alpha \dfrac{\partial F_y}{\partial x} \Delta x + \alpha\left(\dfrac{\partial F_y}{\partial y} - k\right)\Delta y - \beta \Delta\dot{y}. \end{cases} \tag{6}$$

If $U = (\Delta x, \Delta\dot{x}, \Delta y, \Delta\dot{y})^T$, equation (6) can be expressed in matrix form as

$$\begin{cases} \dot{U} = A(\tau)U \\ A(\tau) = A(\tau + 2\pi) \end{cases} \tag{7}$$

TABLE 1

Characteristics of the rub-impact rotor system at different rotating speeds

ω/ω_c	λ_1	λ_2	λ_3	λ_4	Conclusion
2·0	0·0671 + 0·1340i	0·0671 − 0·1340i	−0·0777 + 0·1327i	−0·0777 − 0·1327i	Periodic solution is stable
5·4	−0·4710	0·0087 + 0·4967i	0·0087 − 0·4967i	−0·5269	Periodic solution is stable
6·2	−2·9987	0·1786 + 0·5141i	0·1786 − 0·5141i	−0·0989	Period-doubling bifurcation
8·0	−5·0009	0·3660 + 0·5056i	0·3660 − 0·5056i	−0·0779	Period-doubling bifurcation
14·8	0·7548 + 0·1669i	0·7548 − 0·1669i	−0·4477 + 0·6353i	−0·4477 − 0·6353i	Periodic solution is stable

where

$$A(\tau) = \begin{bmatrix} 0 & 1 & 0 & 0 \\ \alpha\left(\dfrac{\partial F_x}{\partial x} - k\right) & -\beta & \alpha\dfrac{\partial F_x}{\partial y} & 0 \\ 0 & 0 & 0 & 1 \\ \alpha\dfrac{\partial F_y}{\partial x} & 0 & \alpha\left(\dfrac{\partial F_y}{\partial y} - k\right) & -\beta \end{bmatrix}.$$

Equation (7) is a linear homogeneous ordinary differential equation with periodic coefficients. The Floquet theory can be used to analyze bifurcation and stability of the equations.

$\Phi(t)$ is assumed as the basic solution matrix of equation (7) and it has $\Phi(0) = I$. According to the basic theorem of linear ordinary differential equations, there exists a non-singular constant matrix $C = \mathrm{e}^{2\pi R}$ which satisfies $\Phi(t + 2\pi) = \Phi(t)C$. When $t = 0$, $\Phi(0) = I$ and this leads to $C = \Phi(2\pi)$. Therefore, the monodromy matrix C can be produced by integrating the first equation of equations (7) numerically four times, in sequence, obtaining each time a solution $\{\varphi^{(j)}(t)\}$ corresponding to a column matrix of initial conditions with all its elements equal to zero except the element in the jth row, which is equal to 1, and evaluating the solutions at $t = 2\pi$ [16]. Eigenvalues λ_1, λ_2, λ_3 and λ_4 of matrix C are called the characteristic multipliers of the system. Concerning bifurcation and stability of equation (3) there are the following conclusions: (1) When $|\lambda_i| < 1 (i = 1, 2, \ldots, n$ and $n_s = \infty)$, the stable periodic solution of equation (3) is asymptotically stable. (2) If there is one λ_j which passes the unit circle outwards through the point of -1 and other $|\lambda_i|_{i \neq j} < 1$ $(i = 1, 2, \ldots, n)$, the stable periodic solution will have the period-doubling bifurcation. (3) If there is one λ_j which passes the unit circle outwards through the point of $+1$ and other $|\lambda_i|_{i \neq j} < 1$ $(i = 1, 2, \ldots, n)$, the stable periodic solution will have the saddle-node bifurcation. (4) If there is a pair of conjugate complex characteristic multipliers $\lambda_j = a \pm ib$ which pass the unit circle outwards and other $|\lambda_i|_{i \neq j} < 1$ $(i = 1, 2, \ldots, n)$, the stable periodic solution will have the Hopf bifurcation or second Hopf bifurcation and the bifurcation will lead to an invariant torus.

The characteristic multipliers at different rotating speeds of ω/ω_c are shown in Table 1 where $\omega_c = \sqrt{k/m}$ and four harmonic coefficients are retained for each of the displacements, x and y.

It can be seen from the above qualitative analysis that the system of equation (3) does have the period-doubling bifurcation at some rotating speeds. Therefore, the system will become unstable at high rotating speeds and may lead to chaos.

4. NUMERICAL SIMULATION OF CHAOTIC BEHAVIOUR

Equation (3) is a non-linear and non-autonomous system. When the partial rub happens, partial derivatives of the non-linear terms F_x and F_y to x and y do not exist because of the piecewise feature. However, the one-step method to numerically integrate the initial value problem of the ordinary differential equation is convergent as soon as the Lipshitz condition is satisfied. In the following numerical integration the fourth-order Runge–Kutta method is used with chosen $N = 1$. Equation (3) can then be re-written as

$$\begin{cases} \dot{x}_1 = x_2 \\ \dot{x}_2 = \dfrac{1}{m\omega^2} F_x(x_1, y_1) - \dfrac{c}{m\omega} x_2 - \dfrac{k}{m\omega^2} x_1 + U\cos\tau \\ \dot{y}_1 = y_2 \\ \dot{y}_2 = \dfrac{1}{m\omega^2} F_y(x_1, y_1) - \dfrac{c}{m\omega} y_2 - \dfrac{k}{m\omega^2} y_1 + U\sin\tau - \dfrac{g}{\omega^2}. \end{cases} \tag{8}$$

The right-side terms are the periodic functions with the period being 2π. During the calculation a smaller integration step has to be chosen to ensure a stable solution and to avoid the numerical divergence at the point where derivatives of F_x and F_y are discontinuous. Generally long time-marching computation is needed to obtain a convergent orbit. Poincare's map is now used to investigate the stability and the bifurcation characteristics of periodic orbits in equation (8). When the numerical integration is performed to $\tau = 2k\pi$ $(k = 1, 2, \ldots)$, the point sequence obtained is generally called Poincare's maps. Figures of Poincare's map and motion orbit after thousands of periods of integration indicate that the system has the grazing bifurcation, and quasi-periodic and chaotic motions as shown in Figures 3–12. It has to be pointed out that in the figures presented in this paper data of 50 periods are used in all orbit plots and the different scales are used in both the orbit plots and the Poincare's maps in order to amplify the orbits and the attractors. Also the motion of the system, in the form of x/δ and y/δ, is recorded to form orbits and corresponding Poincare's maps and bifurcation diagrams.

The parameter values used in the computation are as follows: mass $m = 4$ kg, damping coefficient $c = 0{\cdot}12 \times 10^4$ N·s/m, stiffness coefficient $k = 0{\cdot}25 \times 10^6$ N/m, impact stiffness

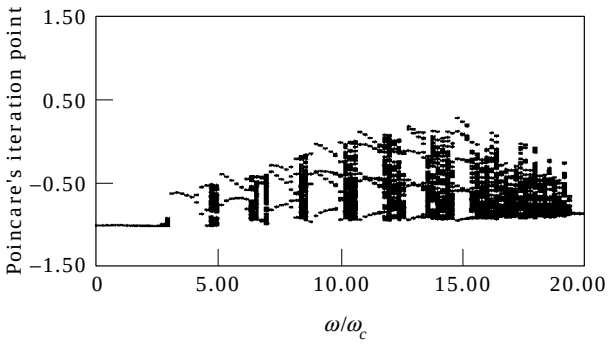

Figure 3. Bifurcation diagram by using ω/ω_c as the control parameter.

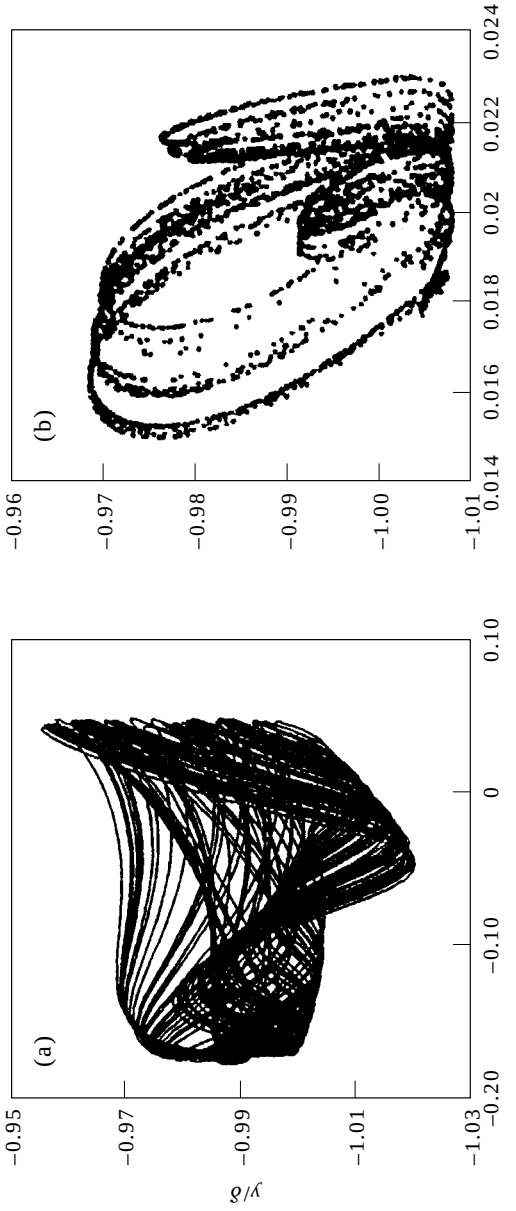

Figure 4. Orbit (a) and Poincaré's map (b) for $\omega/\omega_c = 2{\cdot}7498$.

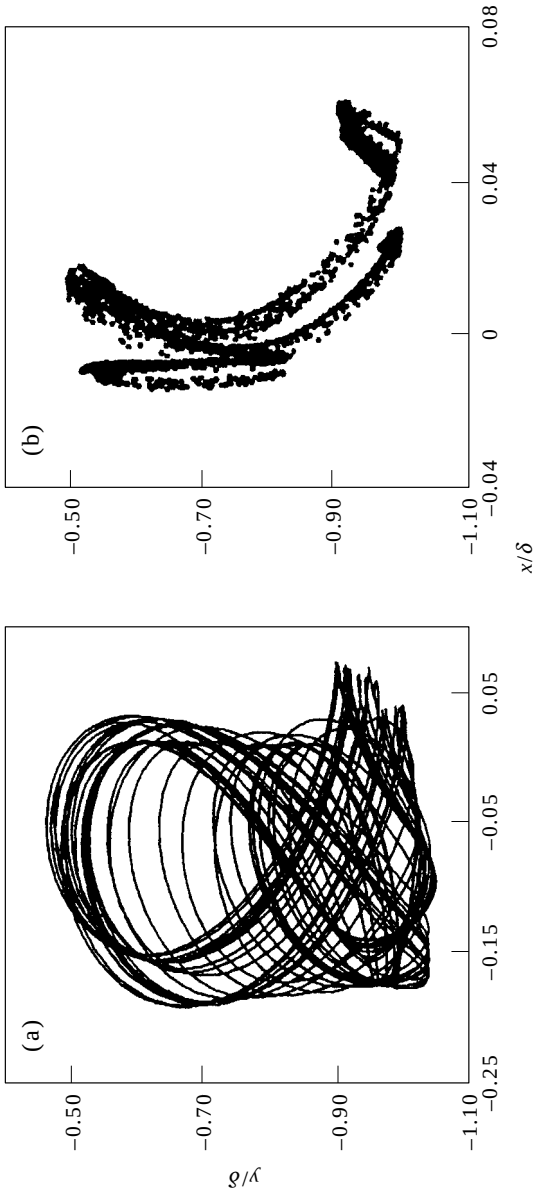

Figure 5. Orbit (a) and Poincare's map (b) for $\omega/\omega_c = 4{\cdot}9$.

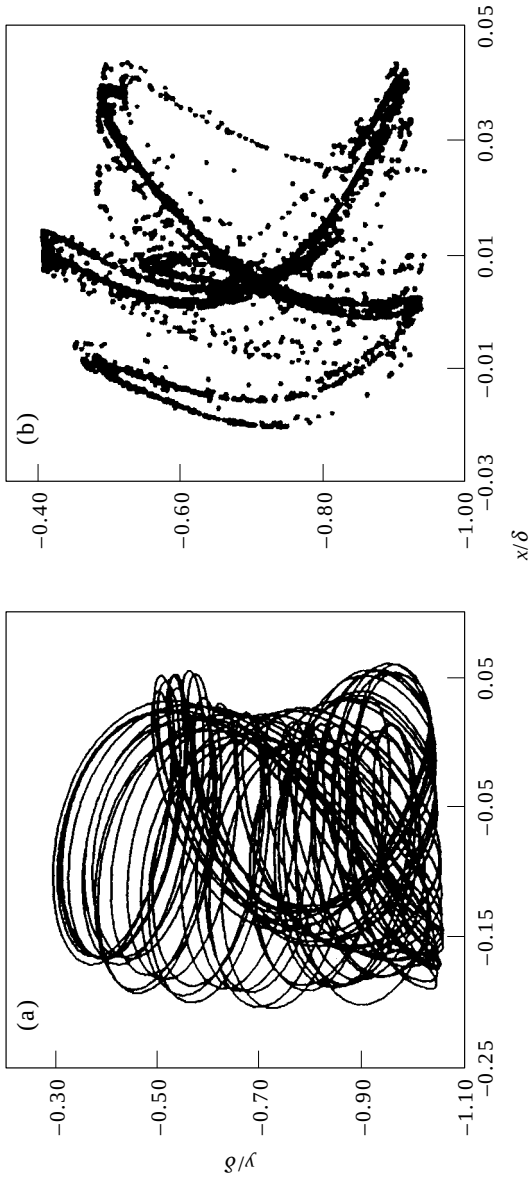

Figure 6. Orbit (a) and Poincare's map (b) for $\omega/\omega_c = 6{\cdot}5$.

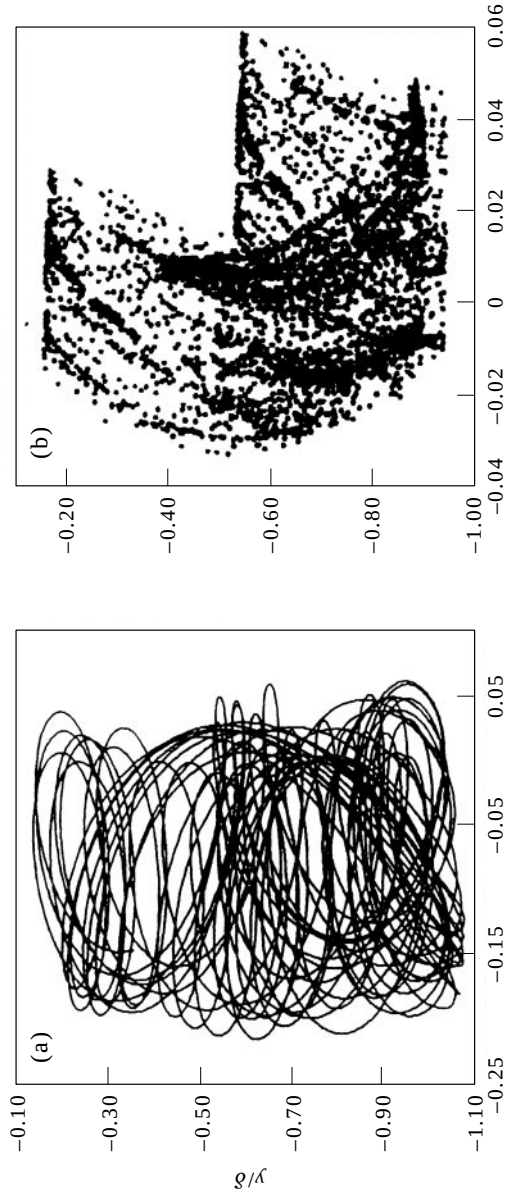

Figure 7. Orbit (a) and Poincare's map (b) for $\omega/\omega_c = 8{\cdot}5$.

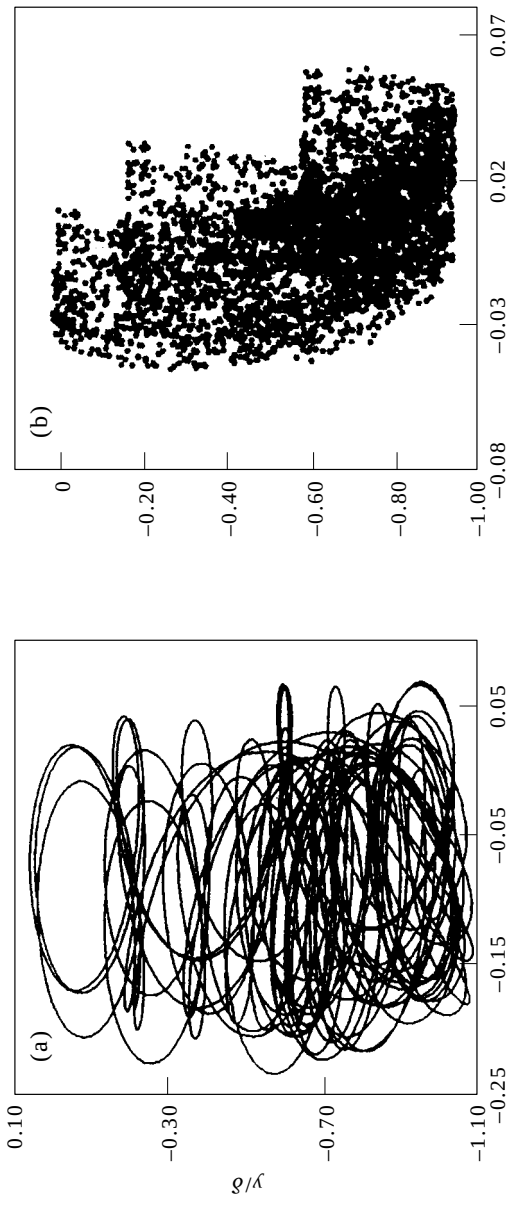

Figure 8. Orbit (a) and Poincare's map (b) for $\omega/\omega_c = 10{\cdot}5$.

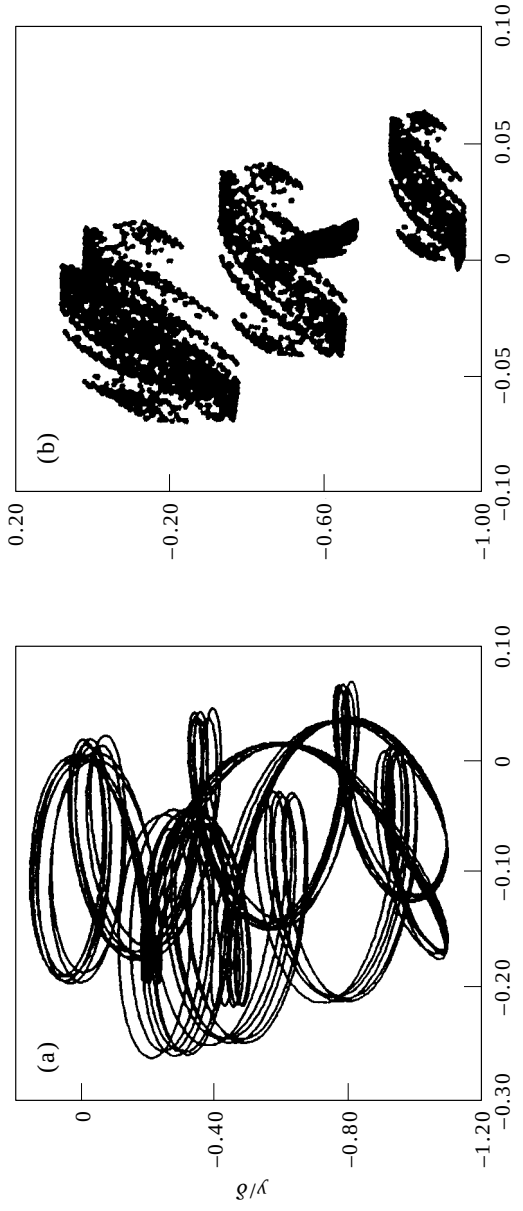

Figure 9. Orbit (a) and Poincare's map (b) for $\omega/\omega_c = 11{\cdot}7$.

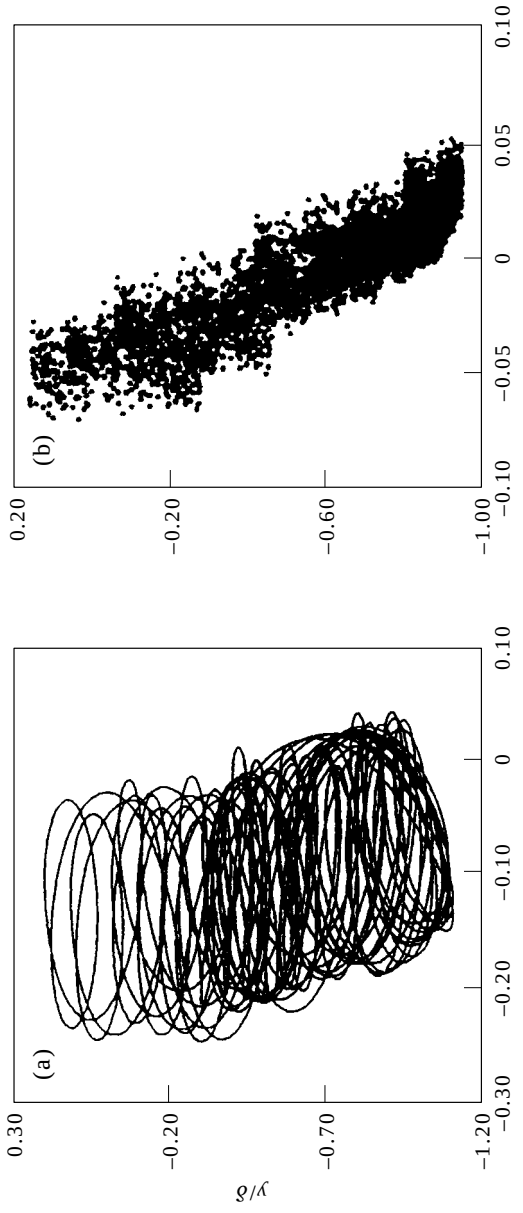

Figure 10. Orbit (a) and Poincare's map (b) for $\omega/\omega_c = 13{\cdot}7$.

TABLE 2

Different forms of motion at different rotating speeds

ω/ω_c	2·5935246	2·5935247	2·61202254	2·61202255	2·73233701
Motion	p2	chaos	chaos	p1	p1
ω/ω_c	2·73233702	2·7498687	2·7498688	2·83000001	2·83000002
Motion	chaos	chaos	p4	p10	chaos

coefficient $k_c = 0{\cdot}6 \times 10^8$ N/m, imbalance $U = 0{\cdot}1 \times 10^{-4}$ m, and friction coefficient $f = 0{\cdot}2$.

Figure 3 is the bifurcation diagram obtained by using the rotating speed as the control parameter. The horizontal axis is ω/ω_c where $\omega_c = \sqrt{k/m}$, the undamped natural frequency of the system. It can be seen from the figure that at very low rotating speeds system vibration is period-one (p1) motion. From about $\omega/\omega_c = 2{\cdot}6$, motion enters into a region of chaos. During this short interval of rotating speeds the chaotic motions exhibit very rich forms and have many different shapes of Poincare's maps. Figure 4 is a typical picture of orbit and Poincare's map in which $\omega/\omega_c = 2{\cdot}7498$. At around $\omega/\omega_c = 3{\cdot}0$ the motion again becomes p1, and then p2 and p3. From $\omega/\omega_c = 4{\cdot}5$ the system gradually enters into another region of chaos. Figure 5 is the typical picture with ω/ω_c being 4·9. After this region the motion immediately becomes p2 and then p4. From about $\omega/\omega_c = 6{\cdot}4$ there exists another region of chaos in which Figure 6 is a representative picture. In this figure the Poincare's map looks like a loosely extended result of that in Figure 5. Then the motion is again periodic with a feature from p3 to p6. At about $\omega/\omega_c = 8{\cdot}4$, the motion has another chaos and a typical orbit and Poincare's map is shown in Figure 7 where $\omega/\omega_c = 8{\cdot}5$. After this the motion is p4. Between $\omega/\omega_c = 10{\cdot}0 \sim 10{\cdot}5$ the motion is chaotic and the fold of the Poincare's map can be seen from Figure 8. From about $\omega/\omega_c = 10{\cdot}6$, the motion becomes p5. At around $\omega/\omega_c = 11{\cdot}5$, the system re-enters into chaos. A typical figure of this region is shown in Figure 9 where the Poincare's map is divided into three parts and the fold can be clearly seen. From about $\omega/\omega_c = 12{\cdot}6$ the motion becomes p6 and gradually p12. And then another region of chaos appears. In Figure 10 where $\omega/\omega_c = 13{\cdot}7$ the Poincare's map has a very confusing shape without any regular fold. From the above analysis it can be seen that the motion of system alternates between periodic vibration and chaos. After a region of chaos the period increases by a value of one. This alternation between periodic motion and chaotic motion and the period-increasing phenomenon are a type of important grazing bifurcation [15].

The routes to and out of chaos can now be investigated. As analyzed above between $\omega/\omega_c = 2{\cdot}6 \sim 3{\cdot}0$, motion is very complicated and has many different forms. At $\omega/\omega_c = 2{\cdot}5935246$ it is a p2 motion and when $\omega/\omega_c = 2{\cdot}5935247$ the motion becomes chaotic. It is reasonable to consider the route to be a sudden transition from periodic vibration to chaos. During this interval of rotating speeds the change in motion can be seen from Table 2. All routes to and out of chaos contained in Table 2 are in the sudden transition between periodic motion and chaos. In the region of chaos located at around $\omega/\omega_c = 5{\cdot}0$, the route to chaos can be seen from Table 3. Clearly this is a period-doubling

TABLE 3

Different forms of motion at different rotating speeds

ω/ω_c	4·60	4·655	4·667	4·6675	4·668	4·67
Motion	p3	p6	p12	p24	p48	chaos

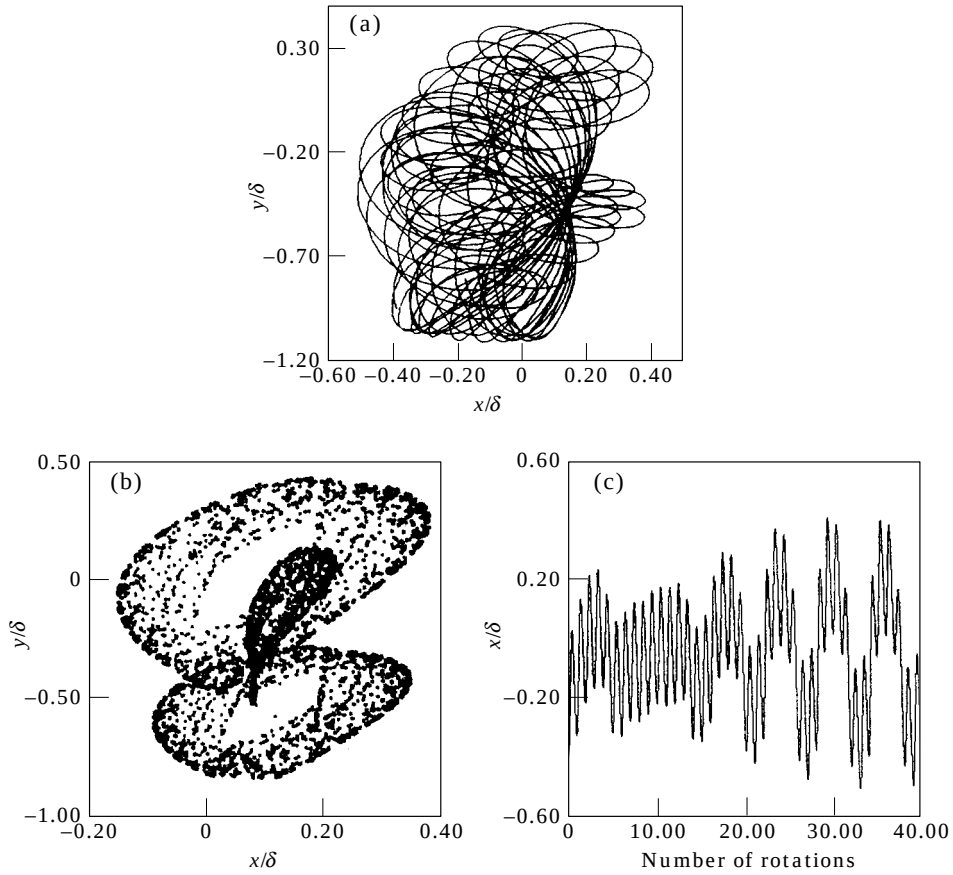

Figure 11. Orbit (a), Poincare's map (b) and motion waveform (c) for $\omega/\omega_c = 7{\cdot}3$.

bifurcation route. In tracing the route out of this region it is found that at $\omega/\omega_c = 5{\cdot}04249945$ motion is chaotic and at $\omega/\omega_c = 5{\cdot}04249950$ motion becomes p2. Therefore this is a route of sudden transition from chaos to periodic motion. In the region of chaos around $\omega/\omega_c = 6{\cdot}5$, the route is also period-doubling bifurcation but in a different format. It follows p2–p4–p8–p16–p32 . . . to chaos.

By increasing U, imbalance, to a new value of $0{\cdot}2 \times 10^{-4}$ m, some interesting results can be observed. Figure 11 shows the orbit, waveform and the Poincare's map for $\omega/\omega_c = 7{\cdot}3$ where the attractor has a shape of butterfly bow and the motion is chaotic. At $\omega/\omega_c = 19{\cdot}3$, quasiperiodic motion is found as shown in Figure 12. The Poincare's map has a closed form.

5.. CONCLUSIONS

In the above calculation and analysis the grazing bifurcation sequence is found in the rub-impact rotor system. This is a special phenomenon caused by the rub-impact process. For the route to chaos, except the usual period-doubling bifurcation as in the one-dimensional dynamical system, there exists a period-increasing feature. This phenomenon can enrich our understanding to chaos and will promote the investigation into bifurcation theory in the rub-impact rotor system and application.

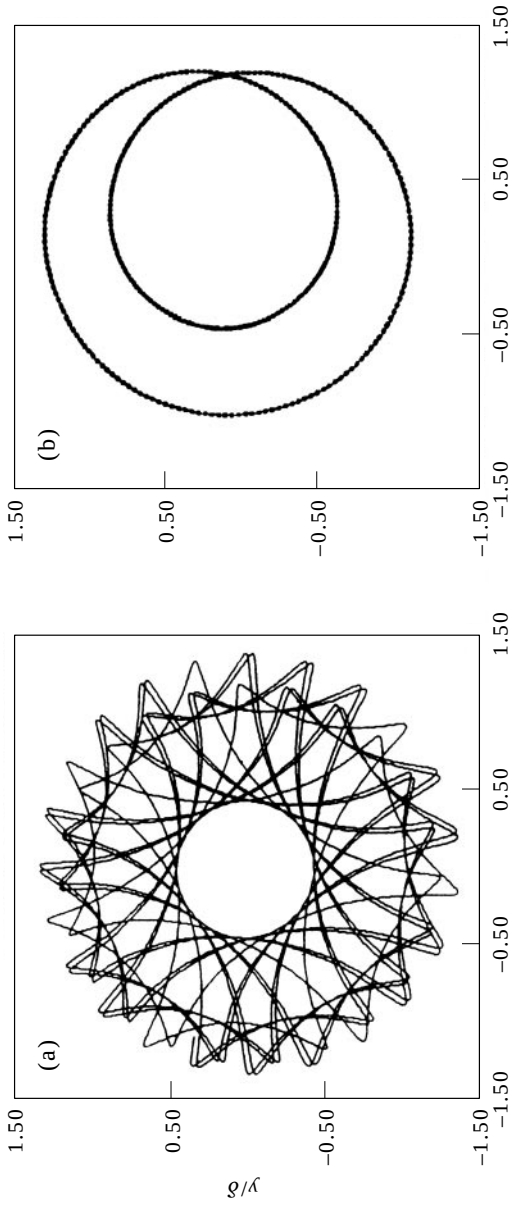

Figure 12. Orbit (a) and Poincaré's map (b) for $\omega/\omega_c = 19{\cdot}3$.

Both the qualitative theoretical analysis and the quantitative numerical calculation indicate that the non-linear rub-impact action caused by the rotor imbalance makes the dynamic characteristics of the system change from the stable periodic motion to the period-doubling bifurcation, the grazing bifurcation, and quasi-periodic and chaotic motion. These results are of great significance to the fault diagnosis of the rub-impact problem.

REFERENCES

1. A. Muszynska 1989 *The Shock and Vibration Digest* **21**(3), 3–11. Rotor-to-stationary element rub-related vibration phenomena in rotating machinery—literature survey.
2. R. F. Beatty 1985 *Transactions of the ASME*, *Journal of Vibration*, *Acoustics*, *Stress*, *and Reliability in Design* **107**, 151–160. Differentiating rotor response due to radial rubbing.
3. F. K. Choy and J. Padovan 1987 *Journal of Sound and Vibration* **113**, 529–545. Non-linear transient analysis of rotor-casing rub events.
4. S. W. Shaw and P. J. Holmes 1983 *Journal of Sound and Vibration* **90**, 129–155. A periodically forced piecewise linear oscillator.
5. J. M. T. Thompson and H. B. Stewart 1986 *Nonlinear Dynamics and Chaos*, *Geometrical Methods for Engineers and Scientists*. Chichester: Wiley.
6. S. K. Choi and S. T. Noah 1994 *Transactions of the ASME*, *Journal of Applied Mechanics* **61**, 131–138. Mode-locking and chaos in a Jeffcott rotor with bearing clearances.
7. Y. B. Kim and S. T. Noah 1990 *Nonlinear Dynamics* **1**, 221–241. Bifurcation analysis for a modified Jeffcott rotor with bearing clearances.
8. Y. S. Choi and S. T. Noah 1987 *Transactions of the ASME*, *Journal of Vibration*, *Acoustics*, *Stress*, *and Reliability in Design* **109**, 255–261. Nonlinear steady-state response of a rotor-support system.
9. R. S. Chancellor, R. M. Alexander and S. T. Noah 1996 *Transactions of the ASME*, *Journal of Vibration and Acoustics* **118**, 375–383. Detecting parameter changes using experimental nonlinear dynamics and chaos.
10. A. Muszynska 1984 *Proceedings of the* 3*rd International Conference on Vibrations in Rotating Machinery*, *Institute of Mechanical Engineers*, *York*, *UK*, 327–335. Partial lateral rotor to stator rubs.
11. M. L. Adams and I. A. Abu-Mahfouz 1994 *Proceedings of IFTOMM* 4*th International Conference on Rotor Dynamics*, *Chicago*, 29–39. Exploratory research on chaos concepts as diagnostic tools for assessing rotating machinery vibration signatures.
12. F. F. Ehrich 1994 *Proceedings of IFTOMM* 4*th International Conference on Rotor Dynamics*, *Chicago*, 1–6. Rotordynamic response in nonlinear anisotropic mounting systems.
13. J. L. Isaksson 1994 *Proceedings of IFTOMM* 4*th International Conference on Rotor Dynamics*, *Chicago*, 85–90. Dynamics of a rotor with annular rub.
14. F. Chu and Z. Zhang 1997 *International Journal of Engineering Science* **35**, 963–973. Periodic, quasi-periodic and chaotic vibrations of a rub-impact rotor system supported on oil film bearings.
15. W. Chin, E. Ott, H. Nusse *et al*. 1994 *Physica Review E* **50**(6), 4427–4444. Grazing bifurcations in impact oscillators.
16. L. Meirovitch 1970 *Methods of Analytical Dynamics*. New York: McGraw-Hill.